Journal of Alloys and Compounds 514 (2012) 113–119

Contents lists available at SciVerse ScienceDirect

Journal of Alloys and Compounds

journal homepage: www.elsevier.com/locate/jallcom

Ferroelectric and nonlinear optical properties of the $LiNbO_3$-type $ZnGeO_3$ from first-principles study

J. Zhang [a,*], B. Xu [a], Z. Qin [a], X.F. Li [a], K.L. Yao [b]

[a] School of Mathematics and Information Science, North China University of Water Resources and Electric Power, ZhengZhou, 450011, China
[b] School of Physics, Huazhong University of Science and Technology, Wuhan, 430074, China

ARTICLE INFO

Article history:
Received 22 August 2011
Received in revised form 2 November 2011
Accepted 3 November 2011
Available online 22 November 2011

Keywords:
First-principles
Spontaneous polarization
Lattice dynamics
Nonlinear optical properties

ABSTRACT

Electronic structure, spontaneous polarization, piezoelectric, and nonlinear optical properties of the $LiNbO_3$(LN)-type $ZnGeO_3$ have been investigated based on the density functional theory. The electronic structure reveals that the LN and corundum-type $ZnGeO_3$ are both direct-band-gap semiconductors. The results reveal that the LN-type $ZnGeO_3$ is ferroelectric with a large spontaneous polarization of 63.59 $\mu C/cm^2$. Although the LN-type $ZnGeO_3$ and $LiNbO_3$ belong to the same point group *3m*, their piezoelectric and nonlinear optical susceptibilities show the different tensor forms. According to the predictive results, the large piezoelectric constants and NLO susceptibilities reveal that the LN-type $ZnGenO_3$ would be a candidate for a high-performance lead-free piezoelectric and nonlinear optical crystal, which will avoid the environmental toxicity problem of the lead-based materials.

1. Introduction

Noncentrosymmetric (NCS) compounds are of significant interest because of their important symmetry-dependent properties, such as dielectricity, piezoelectricity, and second-order nonlinear optical behavior [1–4]. Generally, the basic requirement for ferroelectric property is that the compound must possess a NCS arrangement of the constituent ions and their corresponding electrons. Among the 21 acentric crystal classes, one of the 10 polar point groups (C_1, C_2, C_3, C_4, C_6,C_m. C_{2v}, C_{3v}, C_{4v}, C_{6v}) required for ferroelectric characteristic; in addition, it is noted that piezoelectricity has same symmetry requirement as NLO behavior. In searching for NCS polar oxides, much attention has been paid to oxides including second-order Jahn-Teller distortion cations such as d^0 transition metal ions (Ti^{4+}, Mo^{6+}, etc.) and cations with stereochemical activity of a lone pair electrons of ns^2 (Pb^{2+}, Bi^{3+}, etc.) [5,6].

In 2008, $ZnSnO_3$ as a new $LiNbO_3$ (LN)-type (space group *R3c*, $a = 5.2622$ Å, $c = 14.0026$ Å, $Z = 6$) NCS compound, was synthesized by a solid-state reaction under high pressure at elevated temperature by Inaguma et al. [7]. It was found that $LiNbO_3$-type $ZnSnO_3$ contains only cations with the electronic configuration of $(n-1)d^{10}ns^0$. However, until now little attention has been paid to oxides containing only main-group cations with such electronic configuration, so this compound gave us a new strategy to search for more polar crystals. To search for new high-performance ferroelectric compounds based on the above strategy, we have investigated the possible candidates: $ZnGeO_3$, $CdGeO_3$ and $CdSnO_3$, which have similar structure to $ZnSnO_3$. An interesting question is whether the LN-type $ZnGeO_3$, $CdSnO_3$, and $CdGeO_3$ can be fabricated experimentally. According to the reports in Refs. [8–10], different perovskite-type oxides $A^{2+}B^{4+}O_3$ are compared by using a Goldschmidt diagram, which shows the occurrence of perovskite and $LiNbO_3$ phases as function of A and B cation radius. The Goldschmidt tolerance factor $t = (1/2)^{1/2}(r_A + r_O)/(r_B + r_O)$, where r_A, r_B, and r_O are the ionic radii of A, B cations and O anion, respectively. The Goldschmidt diagram shows that the $LiNbO_3$ phase has tolerance factor less than about 0.78. Therefore, comparing $ZnGeO_3$, $CdGeO_3$ and $CdSnO_3$, it is obvious that only the LN-type $ZnGeO_3$ can be fabricated experimentally.The low pressure phase of $ZnGeO_3$ is ilmenite, which has been confirmed in a sample recovered from high P-T synthesis [11,12]. Based on Ito and Matsui's report [13], the crystal structure of $ZnGeO_3$ underwent a transformation from ilmenite (space group $R\bar{3}$) to corundum (space group $R\bar{3}c$) phase under high temperatures and high pressures. From the crystallographic viewpoint, the $LiNbO_3$ structure is an ordered derivative of the corundum structure in which both A^{2+} and B^{2+} are found in the same layer perpendicular to *c* axis. In Fig. 1(a) and (b), we present the crystal structures of $ZnGeO_3$ in $LiNbO_3$ and corundum-type structures, respectively. According to Yusa et al's report [14], $ZnGeO_3$ ilmenite transformed into perovskite at 30.0 GPa and 1300 ± 150 K in a laser-heated diamond anvil cell. After releasing the pressure, the $LiNbO_3$ phase was recovered as

* Corresponding author. Tel.: +86 0371 69127306.
E-mail address: zhangjing@ncwu.edu.cn (J. Zhang).

0925-8388/$ – see front matter © 2011 Elsevier B.V. All rights reserved.
doi:10.1016/j.jallcom.2011.11.017

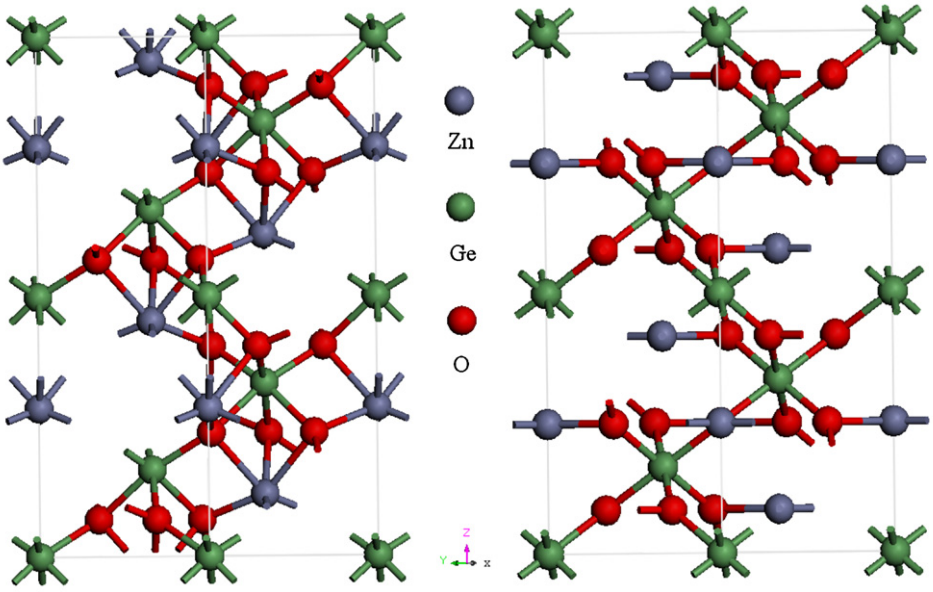

Fig. 1. A view of the crystallographic structure of $ZnGeO_3$ along the *z*-axis: (a) $LiNbO_3$ (LN)-type with the space group *R3c*; (b) corundum-type structure with space group $R\bar{3}c$.

a quenched product. However, until now, as far as we know there are no theoretical studies of LN-type $ZnGeO_3$.

2. Method

In this work, we adopt the ABINIT package [15], a plane-wave pseudopotential (PWPP) density functional theory (DFT) code, which allows not only the usual ground-state calculations but also the linear-response computations of phonon frequency, Born effective charges, spontaneous electric polarization, dielectric, and piezoelectric tensors [16,17]. We perform the geometry optimization and the electronic structure calculations by adopting the ultrasoft pseudopotentials [18]. We use a plane wave cut off of 40 hartrees, with an $8 \times 8 \times 8$ Monkhorst-Pack k-point mesh [19], and the Perdew–Burke–Ernzerhof functional (PBE) [20] of exchange correlation potential both in the generalized gradient approximation (GGA) and local density approximation (LDA). The Zn 4s and 3d electrons, Ge 4s and 4p electrons, as well as O 2s and 2p electrons are considered as valence states in the construction of the pseudopotentials.

In order to obtain the spontaneous polarization, Born effective charges, zone-center phonon modes, dielectric, and piezoelectric tensors, we perform the corresponding linear response computations. The technical details of the computation of responses to atomic displacements, homogeneous electric fields, and strains are based on the density-functional perturbation theory (DFPT) [21–24]. We use norm-conserving pseudopotentials according to the Troullier–Martins scheme [25] with exchange correlation potential in the local density approximation (LDA). In addition, the spontaneous polarization is also calculated with the exchange correlation potential in GGA. We adopt a plane wave cut off of 45 hartrees, and an $8 \times 8 \times 8$ Monkhorst-Pack k-point mesh.

For a material, elastic constants can characterize the ability to deform under small stresses. We can adopt a fourth-rank tensor (C) relating the second-rank stress tensor (σ) to the second-rank strain tensor (η) to describe the elastic constants

$$C_{ij} = \frac{\partial \sigma_i}{\partial \eta_j} \tag{1}$$

where $i, j = 1$–6 indicate the Cartesian coordinate directions with Voigt notation. It is noted that elastic constants are labeled by replacing the pairs of letters *xx*, *yy*, *zz*, *yz*, *zx*, and *xy* by the number 1, 2, 3, 4, 5, and 6 respectively. The elastic constants can be divided into two parts:

$$C_{ij} = \left.\frac{\partial \sigma_i}{\partial \eta_j}\right|_{\mu} + \sum_{\kappa} \frac{\partial \sigma_i}{\partial \mu_i(\kappa)} \frac{\partial \mu_i(\kappa)}{\partial \eta_j} \tag{2}$$

In the above equation: the first part is the clamped ion elastic tensor (C_{clamp}); the second part considering the ionic relaxation effect contains two contributions from force-response internal strain tensors and displacement-response internal strain tensors, and $\mu_i(\kappa)$ is the displacement of atom i along the Cartesian direction κ. The third-rank piezoelectric stress constants (Voigt notation) can be obtained from the zero-field derivative of polarization with respect to strain.

$$e_{\alpha i} = \left.\frac{\partial p_\alpha}{\partial \eta_i}\right|_{E} \tag{3}$$

where $i = 1$–6 indicates the Cartesian directions. The piezoelectric response arises from two parts: the clamped ion response and the contribution from relative displacement of the ionic sublattices.

$$e_{\alpha i} = \left.\frac{\partial p_\alpha}{\partial \eta_i}\right|_{\mu} + \sum_{k} \frac{\partial p_\alpha}{\partial \mu_\alpha(k)} \frac{\partial \mu_\alpha(k)}{\partial \eta_i}. \tag{4}$$

In order to obtain the nonlinear optical susceptibilities and electro-optic (EO) tensors, we carry out the computation of third-order energy derivatives based on $2n+1$ theorem [26]. According to the $2n+1$ theorem, the evaluation of third-order energy derivatives requires no higher-order derivatives of the wave functions than the first one. By minimizing a stationary expression of the second-order energy, we can get the first-order wave functions from linear response. For an insulator, the electric polarization can be expressed as a Taylor expansion of the macroscopic electric field.

$$P_i = P_i^s + \sum_{j=1}^{3} \chi_{ij}^{(1)} \varepsilon_j + \sum_{j,l=1}^{3} \chi_{ijl}^{(2)} \varepsilon_j \varepsilon_l + \ldots, \tag{5}$$

where P_i^s is the zero-field spontaneous polarization, and $\chi_{ij}^{(1)}$ and $\chi_{ijl}^{(2)}$ are the linear dielectric and second-order nonlinear optical susceptibilities, respectively. For the nonlinear optical susceptibility, we only consider the electronic contribution (with the ions at clamped positions) and the third-order derivative of the energy with respect to low-frequency electric fields [26],

$$\chi_{ijl}^{(2)} = -\frac{3}{\Omega_0} E^{\varepsilon_i \varepsilon_j \varepsilon_l} \tag{6}$$

From above definition in Eq. (2), we can obtain the nonlinear optical susceptibility when considering the corresponding low-frequency electric fields as the three perturbations. In addition, it is well-suited to adopt another definition of the nonlinear optical susceptibility d tensor instead of $\chi_{ijl}^{(2)}$.

$$d_{ijl} = \frac{1}{2} \chi_{ijl}^{(2)}. \tag{7}$$

In NCS compounds, the change in the index of refraction n is generally much greater than that in centrosymmetric compounds; it depends linearly on the applied electric field and is known as the electro-optic (or Pockels) effect. The ellipsoid equation and variations of index of refraction n induced by a low-frequency electric field ε_j are described as follows:

$$\left(\frac{1}{n^2}\right)_1 x^2 + \left(\frac{1}{n^2}\right)_2 x^2 + \left(\frac{1}{n^2}\right)_3 x^2 + 2\left(\frac{1}{n^2}\right)_4 yz + 2\left(\frac{1}{n^2}\right)_5 xz + 2\left(\frac{1}{n^2}\right)_6 xy = 1 \tag{8}$$

Table 1
Lattice constants, volume and atomic fractional coordinates of the LN-type (space group *R3c*) and corundum-type (space group $R\bar{3}c$) $ZnGeO_3$.

$ZnGeO_3$ (*R3c*)	*a* (Å)	*c* (Å)	*V* (Å^3)	Zn (0, 0, *z*)	O (*x*, *y*, *z*)
Expt [Ref. 14]	5.0137	13.0211	283.46	0.2214	0.0405, 0.3500, 0.0709
Present (GGA)	5.1007	13.3259	300.26	0.2215	0.0398, 0.3804, 0.0937
Present (LDA)	4.9420	12.8167	271.0950	0.2245	0.0550, 0.3705, 0.0734
$ZnGeO_3$ ($R\bar{3}c$)	*a* (Å)	*c* (Å)	*V* (Å^3)	Zn (0, 0, *z*)	O (*x*, *y*, *z*)
Expt [Ref. 14]	5.0128	13.0219	283.37	0.2500	0.0201, 0.6868, 0.0833
Present (GGA)	5.1167	13.1608	298.40	0.2501	0.0484, 0.6667, 0.0854
Present (LDA)	4.9576	12.6712	269.71	0.2500	0.0507, 0.6775, 0.0833

$$\Delta\left(\frac{1}{n^2}\right)_i = \sum_{j=1}^{3} r_{ij}\varepsilon_j \tag{9}$$

where r_{ij} are the linear EO coefficients (i = 1–6, and j = 1–3). For a ferroelectric material, the EO tensors mainly arise from three components: electronic, ionic and piezoelectric contributions. As discussed in Ref. [26], the electronic contribution comes of the interaction of ε_j with the valence electron when considering the ions as clamped at their equilibrium positions; the ionic contribution comes of the relaxation of the atomic positions to an applied field ε_j; the piezoelectric contribution comes from a relaxation of the unit cell due to the converse piezoelectric effect [27,28].

3. Ground state properties

3.1. Electronic structure

In order to obtain the equilibrium configuration of LN (space group *R3c*) and corundum (space group $R\bar{3}c$) $ZnGeO_3$, we perform the corresponding geometric optimization until the change of the total energy in the self-consistent calculations is less than 10^{-7} eV, and the remaining forces on the atoms are less than 10^{-5} hartrees/bohr. The calculated and experimental results of the lattice parameters for $ZnGeO_3$ are listed in Table 1. According to the obtained lattice parameters, we have calculated their electronic structures along the high symmetry lines. In Fig. 2(a) and (b), we give the corresponding electronic energy band structures of the LN-type and corundum-type $ZnGeO_3$ in GGA, respectively. From the above figure, it is found that the top of the valence band (VB) and the bottom of the conduction band (CB) are both located at G (0, 0, and 0). Therefore, the *R3c* and $R\bar{3}c$ phases $ZnGeO_3$ are direct-band-gap semiconductors. The energy gap (e_g) of $ZnGeO_3$ in *R3c* and $R\bar{3}c$ phases are 1.3 and 1.4 eV, respectively. According to the calculated results in LDA, the energy gap (e_g) of $ZnGeO_3$ in *R3c* and $R\bar{3}c$ phases are 1.6 and 1.7 eV, respectively. In addition, as the well-known underestimation of energy gap based on DFT, the experimental e_g should be larger than the theoretical values.

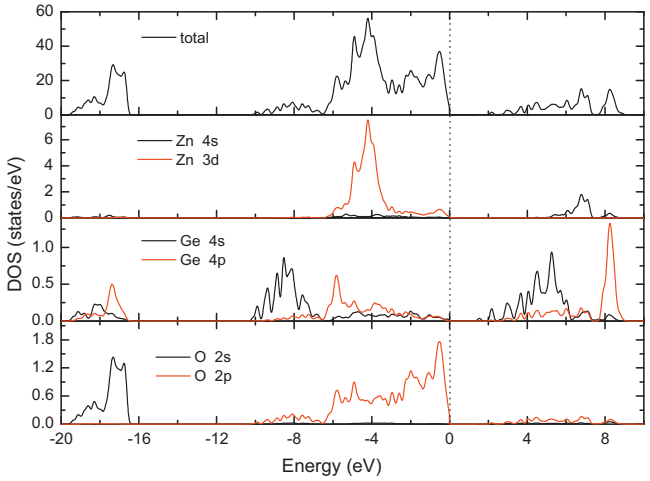

Fig. 3. Total and partial DOS of the LN-type $ZnGeO_3$ in GGA. The Fermi levels are located at 0 eV.

In Fig. 3, we present the total and partial density of states (DOSs) of the LN-type $ZnGeO_3$ in GGA. To further investigate the electronic structure of the LN-type $ZnGeO_3$, we divide the occupied band

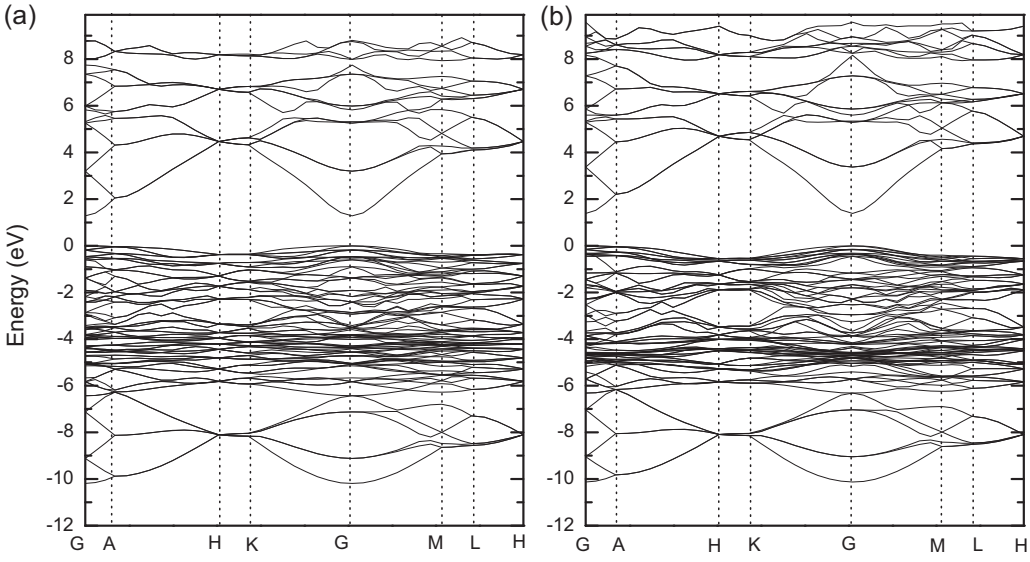

Fig. 2. Band structures $ZnGeO_3$ along the high symmetry directions in the Brillouin zone in GGA: (a) *R3c* phase; (b) $R\bar{3}c$ phase. The Fermi levels are located at 0 eV.

Table 2
Born effective charges (atomic units) of Zn, Ge, O_1, O_2, and O_3 in the LN and corundum-type $ZnGeO_3$ in LDA.

LN-type $ZnGeO_3$ ($R3c$)				Corundum-type $ZnGeO_3$ ($R\bar{3}c$)			
Zn	2.45	0	−0.59	Zn	2.42	0	0
	0	1.99	0.14		0	2.42	0
	−0.59	0.26	2.19		0	0	2.25
Ge	4.28	0.28	0	Ge	4.21	−0.07	0
	−0.28	4.28	0		0.07	4.21	0
	0	0	4.41		0	0	4.19
O_1	−2.13	0.22	−0.17	O_1	−2.09	0.21	−0.46
	0.19	−2.31	0.58		0.21	−2.33	0.80
	−0.06	0.65	−2.19		−0.39	0.69	−2.14
O_2	−2.45	0.01	0.59	O_2	−2.44	0	0.92
	0.03	−1.99	0.14		0	−2.29	0
	0.59	0.26	−2.19		0.79	0	−2.14
O_3	−2.39	0	0	O_3	−2.09	0.21	−0.46
	0	−2.39	0		0.21	−2.33	0.80
	0	0	−2.18		−0.39	0.69	−2.14

structure into the three energy regions: (i) bands lying between −20 and −16 eV, (ii) bands lying between −10 and −6.5 eV, (iii) bands within the range from −6.5 to 0 eV. In Region (i), the bands mainly arise from Ge 4s, 4p and O 2s states, from which we note that the partial DOS of Ge 4p and O 2s have similar peaks and character; Region (ii) includes 12 bands, which mostly come from O 2p, Ge 4s, and with small contribution from Ge 4p. Among them we find that the DOS of O 2p and Ge 4p have similar peaks and character; Region (iii) with the most bands is mainly contributed by Zn 3d, Ge 4s and 4p, and O 2p states, in this region there obviously exists hybridization between Ge 4p-O 2p and Zn 3d-O 2p states. Above the Fermi level, in the energy range from 1.3 to 4 eV, we find that there are only two conduction bands due to the Ge 4s single pair electrons.

Next, to analyze the bonding character of the LN-type $ZnGeO_3$, we perform a calculation of the Mulliken charge population of this compound. The results show that the partial charge distribution of Zn, Sn and O atoms as follows: for Zn atoms, the charge population of the s, p, and d orbitals are 0.50, 0.62, and 9.98, respectively; for Ge atoms, the charge population of the s, p, and d orbitals are 0.91, 1.51 and 0.00, respectively; for O atoms, the charge population of the s, p orbitals are 1.85 and 4.97. In addition, the charge transfer from Zn and Ge to O is about 0.90 and 1.59 e. According to the optimized crystal structure of the LN-type $ZnGeO_3$, the obtained charge populations of the nearest-neighboring (2.006 Å) and the next nearest-neighboring (2.296 Å) Zn–O bonds are 0.42 and 0.13; the charge populations of the nearest-neighboring (1.906 Å) and next nearest-neighboring (1.993 Å) Ge–O bonds are 0.39 and 0.19. We know that a small value of the bond population usually displays ionic character, and a large value of the bond population reveals a covalent bond. Therefore, the chemical bonding of Ge–O and Zn–O bonds is mixed covalent-ionic character.

3.2. Spontaneous polarization

As the Born effective charge tensors can help us to further investigate the origin of the spontaneous polarization, we perform the corresponding linear response calculations to obtain them. It is well known that the atomic charge definitions can be categorized in either static, based on the partitioning of the charge density into contributions to the specific atoms, or Born effective charges (Z^*), defined by the change in polarization created by atomic displacement

$$Z^*_{i,\alpha\beta} = \frac{\Omega}{e}\frac{\partial P_\beta}{\partial u_{i,\alpha}} \tag{10}$$

where Z^* is the polarization per unit cell in the direction β induced by displacement of atomic i in the direction α, and Ω is the primitive cell volume. By calculating the linear response to atomic displacements based on Eq. (10), we obtain the Born effective charge tensors of the LN and corundum-type $ZnGeO_3$. Because Z^* can reflect the covalence of the bonding environment of each atom with respect to its nominal ionic value, we can compare Z^* with the corresponding nominal ionic values. In the following, we mainly discuss the relation between Z^* (Table 2) and spontaneous polarization. For $ZnGeO_3$, the nominal ionic values of Zn, Ge, and O are +2, +4, and −2, respectively. By comparing these ionic values with Z^*, it is found that Z^* of Zn, and O atoms are relatively more anomalous than that of Ge atoms. This anomalism is an important feature also found in other ferroelectric compounds [29–32]. Based on Table 2, in the LN-type (ferroelectric phase) $ZnGeO_3$, it is found that Z^* of Zn, O_1 and O_2 show strong anisotropy, and Z^* of O_3 is nearly isotropic; in the corundum-type (paraelectric phase) $ZnGeO_3$, we find that Z^* of O_1 and O_3 show strong anisotropy, and Z^* of Zn and Ge are nearly isotropic.

The modern theory of polarization developed by Resta [33], King-Smith, and Vanderbilt [34] presents the correct definition to compute the spontaneous polarization from the occupied Bloch eigenvectors of the self-consistent crystalline Hamiltonian [35]. In this work, we have calculated the spontaneous polarizations by finite electric field method based on the Berry phase model. In the finite electric field calculations, firstly, along the different crystal directions, we adopt a series of positive weak homogeneous electric fields as a perturbation to obtain a series of electric polarization until these values tend to saturation. Next, similarly, using a series of negative homogeneous electric fields as perturbation, we can obtain almost the same absolute value of the saturated electric polarization. We use this method to calculate the spontaneous polarization of the $ZnGeO_3$. For a certain material, the total spontaneous polarization is the sum of the ion polarization (P_{ion}) and electronic polarization (P_{ele}). First, we calculate the spontaneous polarization of the LN-type $ZnGeO_3$ along the x, y, and z axes. The calculated spontaneous polarization P_x, P_y, and P_z of $ZnGeO_3$ are 0.89, 0.89, 63.59 μC/cm^2, respectively. These values reveal that polar direction is mainly along the z-axis, which is in accord with the symmetry of the 3m point group. For P_z, the calculated results reveal that the ionic and electronic polarization P_{ion} and P_{ele} are 90.61 and −27.02 μC/m^2, respectively. In addition, the calculated spontaneous polarization of LN-type $ZnGeO_3$ along z-axis is 63.84 μC/m^2, and the corresponding ionic and electronic polarization P_{ion} and P_{ele} are 90.61 and −26.76 μC/m^2, respectively. By investigating the crystal structure of LN-type $ZnGeO_3$, because the cation sequence along the z-axis is Sn–Zn–Vac–Sn–Zn–Vac–Sn...

(Vac = vacancy), the Zn atom is located in a large distorted position. Due to the symmetry breaking of the cations sequences including vacancies, the polarization direction of the LN-type $ZnGeO_3$ is along the *z*-axis. The large spontaneous polarization attributes to the large displacement of Zn atoms because of the mixed ionic-covalent character between the Zn–O bonds.

4. Lattice dynamical properties

4.1. Zone-center phonon modes

In traditional ferroelectrics, such as $BaTiO_3$, $PbTiO_3$ and $LiNbO_3$, etc., the ferroelectricity is driven by the condensation of zone-center soft phonons [36]. First, we perform a symmetry analysis and decompose the symmetry-adapted modes into irreducible representations for $ZnGeO_3$ in their paraelectric and ferroelectric phases, respectively. In the high-symmetry paraelectric phase ($R\bar{3}c$), at the Γ point all the 30 modes, including 3 acoustic modes, are decomposed into 6 representations,

$$\Gamma\left(R\bar{3}c\right) = A_{1g} \oplus 2A_{1u} \oplus 3A_{2g} \oplus 4A_{2u} \oplus 8Eg \oplus 12E_u \quad (11)$$

Among them, the three acoustic modes one in A_{2u} and two E_u modes, and A_{1g} and E_g optical modes are Raman active; A_{2u} and E_u optical modes are infrared (IR) active. Due to the double degeneracy of E_g and E_u, there are A_{1g}, $2A_{1u}$, $3A_{2g}$, $3A_{2u}$, $4E_g$, and $5E_u$ irreducible optical phonons. In the ferroelectric phase ($R3c$), at the Γ point, the total 30 phonons can be decomposed into 3 representations,

$$\Gamma(R3c) = 5A_1 \oplus 5A_2 \oplus 20E. \quad (12)$$

The A_1 and E optical modes are Raman and infrared active, while A_2 are silent. In addition, the acoustic modes with zero frequency are one A_1 modes and two in E modes. Because of the double degeneracy of E modes, there are $4A_1$, $5A_2$, and $9E$ irreducible optical modes in the ferroelectric phase. By analyzing the symmetry character for each irrep of the two different space groups, the E modes are composed of E_g and E_u in the transition from paraelectric to ferroelectric phase.

4.2. Dielectric properties

Combining with the zone-center phonon frequencies and Born effective charges, we have calculated the dielectric constants of $ZnGeO_3$ in the ferroelectric phase. The static dielectric response of the ground state can be decomposed into two parts: the electronic contribution $\varepsilon^{\infty}_{\alpha\beta}$, which can be obtained from the electron gas response, and the lattice contribution obtained from the zone-center polar-phonon frequencies [36] and the undamped harmonic oscillators and are as follows:

$$\varepsilon^{0}_{\alpha\beta} = \varepsilon^{\infty}_{\alpha\beta} + \frac{4\pi}{\Omega_0}\sum_{m}\frac{S_m}{\omega_m^2} \quad (13)$$

where α and $\beta = x, y$, and z are the axis indices, and $S_{m,\alpha\beta} = P_{m\alpha}\cdot P_{m\beta}$ is the mode-oscillator strength, and $P_{m\alpha} = \sum_{k,\gamma} Z^{*}_{k,\gamma\alpha}\xi^{m}_{\kappa\gamma}/\sqrt{M_\kappa}$ is the mode polarity for the phonon with frequency ω_m and eigenvector ξ'''. In addition, the mode effective charges are defined as $Z^{*}_{m,\alpha} = \sum_{k,\gamma} M_k^{1/2} Z^{*}_{k,\gamma\alpha}\xi^{m}_{\kappa\gamma}$. Considering the symmetry, the dielectric tensors along and perpendicular to z axis are different. For the LN-type $ZnGeO_3$, we get the optical dielectric tensors $\varepsilon^{\infty}_{xx} = \varepsilon^{\infty}_{yy} = 5.22$ and $\varepsilon^{\infty}_{zz} = 5.19$. Therefore, the symmetry axis of the LN-type $ZnGeO_3$ is positive uniaxial ($\varepsilon^{\infty}_{zz}/\varepsilon^{\infty}_{zz} < 1$), which is different from but close to $LiNbO_3$ ($\varepsilon^{\infty}_{zz}/\varepsilon^{\infty}_{zz} > 1$). Although the electronic response $\varepsilon^{\infty}_{\alpha\beta}$ in LDA is usually overestimated compared with the experimental values, it is a negligible impact due to the accuracy of the static response is about an order of magnitude larger than the computed electronic response. The obtained static dielectric tensor of ε^{0}_{xx}, ε^{0}_{yy} and ε^{0}_{zz} for the LN-type $ZnGeO_3$ are 21.71, 21.71, 40.13, respectively. The transverse optical mode frequencies ω_m, mode effective charges, and the mode-oscillator strength $S_{m,\alpha\beta}$ of mode m of the LN-type $ZnGeO_3$ are presented in Table 3. For the static dielectric tensor ε^{0}_{xx} and ε^{0}_{yy}, we observe that two E modes (263.96 and 387.16 cm^{-1}) with large mode effective charge and oscillator strength make a major contribution, meanwhile, a small contributions arise from three E modes (200.33, 240.46, and 328.32 cm^{-1}); for ε^{0}_{zz}, the most important contributions originate from one E mode (190.29 cm^{-1}), which has the largest mode effective charge and oscillator strength among all the modes.

Table 3
The calculated frequencies (cm^{-1}), mode effective charges ($|e|$), and mode-oscillator strengths (in 10^{-4} atomic units) of active transverse optical phonon modes of the LN-type $ZnGeO_3$.

A_1 modes ($ZnGeO_3$)			E modes ($ZnGeO_3$)		
ω	Z_m^{*}	S_m	ω	Z_m^{*}	S_m
164.44	3.13	1.24	182.12	2.41	0.58
190.29	7.19	11.98	200.33	3.28	1.21
503.10	1.39	0.66	240.46	2.77	1.61
533.38	1.30	0.58	263.96	3.52	3.87
			303.61	0.90	0.22
			328.32	2.16	1.13
			387.16	4.09	5.19
			543.70	0.82	0.22
			613.21	0.61	0.13

Table 4
Elastic stiffness constants of the LN-type $ZnSnO_3$ and $ZnGeO_3$.

	Elastic stiffness tensors C_{ij} (10^{11} N/m^2)						
	C_{11}	C_{12}	C_{13}	C_{15}	C_{33}	C_{44}	C_{66}
$ZnSnO_3$	1.94	0.63	1.01	0.001	1.69	1.17	0.92
$ZnGeO_3$	1.81	0.93	0.55	0.20	1.76	0.46	0.44
	C_{11}	C_{12}	C_{13}	C_{14}	C_{33}	C_{44}	C_{66}
$LiNbO_3$ [Ref. 39]	2.03	0.53	0.75	0.09	2.45	0.60	0.75
$LiTaO_3$ [Ref. 39]	2.298	0.440	0.812	−0.104	2.798	0.968	0.929

4.3. Piezoelectric properties

By treating homogeneous strain within the density-functional perturbation theory, we have investigated the elastic and piezoelectric properties of these compounds. The obtained elastic constants of these compounds have seven independent nonzero elements (Voigt notation) C_{11}, C_{12}, C_{13}, C_{15}, C_{33}, C_{44}, and C_{66}:

$$C = \begin{pmatrix} C_{11} & C_{12} & C_{13} & 0 & C_{15} & 0 \\ C_{12} & C_{11} & C_{13} & 0 & -C_{15} & 0 \\ C_{13} & C_{13} & C_{33} & 0 & 0 & 0 \\ 0 & 0 & 0 & C_{44} & 0 & -C_{15} \\ C_{15} & -C_{15} & 0 & 0 & C_{44} & 0 \\ 0 & 0 & 0 & -C_{15} & 0 & C_{44} \end{pmatrix} \quad (14)$$

The relaxed-ion elastic stiffness tensors are presented in Table 4. Due to $C_{66} = (C_{11} - C_{12})/2$, the number of independent elements reduce to six. According to the Born mechanical stability criterion [37,38] of the triangle crystal, the restriction can be expressed as follows:

$$\begin{aligned} &C_{11} - \left|C_{12}\right| > 0 \\ &(C_{11} + C_{12})C_{33} - 2C_{13}^2 > 0\,. \\ &(C_{11} - C_{12})C_{44} - 2C_{15}^2 > 0 \end{aligned} \quad (15)$$

Table 5
Piezoelectric stress constants of the LN-type $ZnSnO_3$ and $ZnGeO_3$.

Piezoelectric stress constants e_{ij} (C/m^2)				
	e_{11}	e_{15}	e_{31}	e_{33}
$ZnSnO_3$	−0.15	0.26	1.23	0.29
$ZnGeO_3$	−0.27	0.36	0.65	2.81
	e_{22}	e_{15}	e_{31}	e_{33}
$LiNbO_3$ [Ref. 39]	2.43	3.76	0.23	1.33
$LiTaO_3$ [Ref. 39]	1.67	2.72	−0.38	1.09

Based on the data in Table 4, the two compounds all satisfy the Born stability restrictions, which reveal that these materials are mechanically stable. It is well known that the two typical ferroelectric crystal $LiNbO_3$ and $LiTaO_3$ belong to the 3m point group (space group *R3c*), the six independent elastic constants are C_{11}, C_{12}, C_{13}, C_{14}, C_{33}, and C_{44} ($2C_{66} = C_{11} - C_{12}$). Comparing the elastic constants of $ZnGeO_3$ with those of $LiNbO_3$ and $LiTaO_3$ [39], we also list their elastic stiffness constants in Table 4. In addition, according to the calculated results, the piezoelectric stress constants of these compounds have 4 independent nonzero elements (Voigt notation) e_{11}, e_{15}, e_{31}, e_{33}:

$$e = \begin{pmatrix} e_{11} & -e_{11} & 0 & 0 & e_{15} & 0 \\ 0 & 0 & 0 & e_{15} & 0 & 0 \\ e_{31} & e_{31} & e_{33} & 0 & 0 & 0 \end{pmatrix}. \quad (16)$$

The obtained relaxed-ion piezoelectric stress tensors of $ZnSnO_3$ and $ZnGeO_3$ are in Table 5. The large piezoelectric stress constants reveal that these four compounds are promising lead-free piezoelectric. For $LiNbO_3$ and $LiTaO_3$, the four independent (Voigt notations) elements are e_{15}, e_{22}, e_{31}, and e_{33}:

$$e = \begin{pmatrix} 0 & 0 & 0 & 0 & e_{15} & 0 \\ -e_{22} & e_{22} & 0 & e_{15} & 0 & 0 \\ e_{31} & e_{31} & e_{33} & 0 & 0 & 0 \end{pmatrix} \quad (17)$$

In Table 5, we also present the corresponding piezoelectric stress tensors of $LiNbO_3$ and $LiTaO_3$. By comparing piezoelectric coefficients of LN-type $ZnSnO_3$ and $ZnGeO_3$ with that of $LiNbO_3$ and $LiTaO_3$, it is found that the piezoelectric stress tensors of these compounds have four independent nonzero elements e_{11}, e_{15}, e_{31}, e_{33}; while for $LiNbO_3$ and $LiTaO_3$ the four independent piezoelectric constants are e_{15}, e_{22}, e_{31}, and e_{33}. Although the LN-type $ZnSnO_3$ and $ZnGeO_3$ and the typical ferroelectric $LiNbO_3$ belong to the same point group (3m), the piezoelectric coefficients present the different tensor forms.

5. Nonlinear optical properties

As the space group of LN-type $ZnGeO_3$ is *R3c*, which belongs to the point group 3m, this compound is a candidate nonlinear optical (NLO) material. Based on density-functional perturbation theory, we have calculated the NLO susceptibilities and electro-optic (EO) tensor of the LN-type $ZnGeO_3$. In this work, we do not consider the impact of energy band gap correction because of a lake of experimental data of the energy gap and nonlinear optical properties. According to our previous study [40], the NLO susceptibilities of LN-type $ZnSnO_3$ have 4 independent elements (Voigt notations) d_{12}, d_{31}, d_{15}, d_{33}.

$$d = \begin{pmatrix} -d_{12} & d_{12} & 0 & 0 & d_{15} & 0 \\ 0 & 0 & 0 & d_{15} & 0 & d_{12} \\ d_{31} & d_{31} & d_{33} & 0 & 0 & 0 \end{pmatrix} \quad (18)$$

By using kleinman's symmetry [41,42], this tensor has three independent elements because of $d_{31} = d_{15}$. Based on our calculated results, it is found that the LN-type $ZnSnO_3$ and $ZnGeO_3$ have the same tensor of NLO susceptibilities and EO coefficients. The obtained values of the three independent elements d_{12}, d_{31}, and d_{33} for the LN-type $ZnGeO_3$ are 3.14, 6.16, and 8.45 pm/V, respectively. The total EO tensor (Voigt notations) of the LN-type $ZnGeO_3$, the obtained has four independent elements γ_{11}, γ_{13}, γ_{33}, and γ_{51}.

$$\gamma = \begin{pmatrix} \gamma_{11} & 0 & \gamma_{13} \\ -\gamma_{11} & 0 & \gamma_{13} \\ 0 & 0 & \gamma_{33} \\ 0 & \gamma_{51} & 0 \\ \gamma_{51} & 0 & 0 \\ 0 & -\gamma_{11} & 0 \end{pmatrix} \quad (19)$$

The values obtained for γ_{11}, γ_{13}, γ_{33}, and γ_{51} in LN-type $ZnGeO_3$ are 0.44, 1.68, 5.56 and 0.85, respectively. It is noted that, in $LiNbO_3$, the matrix elements of NLO susceptibilities and EO tensor are d_{22}, d_{31}, d_{33}, d_{15} ($d_{15} = d_{31}$) and γ_{13}, γ_{33}, γ_{22} and γ_{51}; however in $ZnGeO_3$, they are d_{12}, d_{31}, d_{33}, d_{15} ($d_{15} = d_{31}$) and γ_{11}, γ_{13}, γ_{33} and γ_{51}. Although the point group of LN-type $ZnGeO_3$ and $LiNbO_3$ is same (3m), by comparing the nonlinear optical properties of the two compounds, it is found that the NLO susceptibilities and EO coefficients of $LiNbO_3$ ($m \perp x_1$) and $ZnGeO_3$ ($m \perp x_2$) show different tensor forms [43]. The large NLO susceptibilities indicate that the LN-type $ZnGeO_3$ is a promising nonlinear optical material.

6. Conclusions

Based on density functional theory (DFT), we have investigated the electronic structure, spontaneous polarization, piezoelectric, and nonlinear optical properties of the LN-type $ZnGeO_3$ The electronic structure reveals that the LN (space group *R3c*) and corundum-type $ZnGeO_3$ are both direct-band-gap semiconductors, and the energy gaps (e_g) are 1.3 and 1.4 eV, respectively. The spontaneous polarization (P_s) shows that LN-type $ZnGeO_3$ is ferroelectric with large P_s of 63.59 μC/m^2. Due to the symmetry breaking of the cations sequences including vacancies, the polarization direction of the LN-type $ZnGeO_3$ is along the z-axis. The large spontaneous polarization attributes to the large displacement of Zn atoms because of the mixed ionic-covalent character between the Zn–O bonds.

By analyzing the Zone-center phonon modes of the ferroelectric and paraelectric phases for $ZnGeO_3$, it is found that the three zero frequency acoustic modes are the one in A_1 and two in E modes in the ferroelectric phase; in the transition from paraelectric to ferroelectric phase the E modes are composed of E_g and E_u. Using homogeneous strain within the density-functional perturbation theory, we have calculated the elastic and piezoelectric properties of LN-type $ZnGeO_3$. The elastic constants of this compound satisfy the Born stability restrictions, which reveal that they are mechanically stable. The piezoelectric stress constants e_{31} and e_{33} of the LN-type $ZnGeO_3$ are 1.23 and 0.29 C/m^2, respectively. Comparing nonlinear optical properties of LN-type $ZnGenO_3$ with that of $LiNbO_3$, although the two compounds belong to the same point group (3m), it is found that the NLO susceptibilities and EO coefficients show the different tensor forms.

According to the above predictive results, the large piezoelectric constants and NLO susceptibilities reveal that the LN-type $ZnGenO_3$ would be a candidate for a high-performance lead-free piezoelectric and nonlinear optical crystal, which make it avoid the environmental toxicity problem of the lead-based materials.

Acknowledgments

This work was supported by China 973 plan (no. 2006CB921605), the National Natural Science Foundations of China (nos. 11104072, 10804034, and 10774051) and the Research

Fund for the Doctoral Program of Higher Education of China (no. 20090142110063).

References

[1] P.S. Halasyamani, K.R. Poeppelmeier, Chem. Mater. 10 (1998) 2753.
[2] O. Auciello, J.F. Scott, R. Ramesh, Phys. Today 51 (1998) 22.
[3] A. Frau, J.H. Kim, P.S. Halasyamani, Solid State Sci. 10 (2008) 1263.
[4] H.Y. Chang, S.H. Kim, P.S. Halasyamani, K.M. Ok, J. Am. Chem. Soc. 131 (2009) 2426.
[5] P.S. Halasyamani, Chem. Mater. 16 (2004) 3586.
[6] J.H. Kim, P.S. Halasyamani, J. Solid State Chem. 181 (2008) 2108.
[7] Y. Inaguma, M. Yoshida, T. Katsumata, J. Am. Chem. Soc. 130 (2008) 6704.
[8] K. Leinenweber, W. Utsumi, Y. Tsuchida, T. Yagi, K. Kurita, Phys. Chem. Miner. 18 (1991) 244.
[9] J. Linton, Y. Fei, A. Navrotsky, Am. Mineralogist 84 (1999) 595.
[10] A. Navrotsky, Chem. Mater. 10 (1998) 2787.
[11] A.E. Ringwood, A. Major, Nature 215 (1967) 1367.
[12] Y. Syono, S. Akimoto, Y. Matsui, J. Solid State Chem. 3 (1971) 369.
[13] E. Ito, Y. Matsui, Phys. Chem. Miner. 4 (1979) 265.
[14] H. Yusa, M. Akaogi, N. Sata, H. Kojitani, R. Yamamoto, Y. Ohishi, Phys. Chem. Miner. 33 (2006) 217.
[15] The ABINIT code is a common project of the University Catholique de Louvain, Corning Incorporated, and other contributions (http://www.abinit.org).
[16] X. Gonze, C. Lee, Phys. Rev. B 55 (1997) 10355.
[17] X. Gonze, Phys. Rev. B 55 (1997) 10337.
[18] D. Vanderbilt, Phys. Rev. B 41 (1990) 7892.
[19] H.J. Monkhorst, J.D. Pack, Phys. Rev. B 13 (1976) 5188.
[20] J.P. Perdew, K. Burke, M. Ernzerhof, Phys. Rev. Lett. 77 (1996) 3865.
[21] S. Baroni, S. de Gironcoli, A. Dal Corso, Rev. Mod. Phys. 73 (2001) 515.
[22] S. Baroni, P. Giannozzi, A. Testa, Phys. Rev. Lett. 58 (1987) 1861.
[23] R. Shaltaf, X. Gonze, M. Cardona, R.K. Kremer, G. Siegle, Phys. Rev. B 79 (2009) 075204.
[24] R. Shaltaf, E. Durgun, J.-Y. Raty, Ph. Ghosez, X. Gonze, Phys. Rev. B 78 (2008) 205203.
[25] N. Troullier, J.L. Martins, Phys. Rev. B 43 (1991) 1993.
[26] M. Veithen, X. Gonze, Ph. Ghosez, Phys. Rev. B 71 (2005) 125107.
[27] M. Veithen, X. Gonze, Ph. Ghosez, Phys. Rev. Lett. 93 (2004) 187401.
[28] S.H. Wemple, D. DiDomomenico Jr., in: R. Wolfe (Ed.), Applied Solid State Science, Academic, New York, 1972.
[29] Z. Li, J. Yang, J.G. Hou, Q. Zhu, Phys. Rev. B 70 (2004) 144518.
[30] Kwan-Woo Lee, W.E. Pickett, Phys. Rev. B 68 (2003) 085308.
[31] U. Waghmare, H.F. Marcel, T. Sluiter, T. Kimura, Y. Goto, Y. Kawazoe, Appl. Phys. Lett. 84 (2004) 4917.
[32] G. Geneste, J.M. Kiat, C. Malibert, J. Chaigneau, Phys. Rev. B 75 (2007) 174107.
[33] R. Resta:, Rev. Mod. Phys. 66 (1994) 899.
[34] R.D. King-Smith, D. Vanderbilt, Phys. Rev. B 47 (1993) 1651;
D. Vanderbilt, R.D. King-Smith, Phys. Rev. B 48 (1993) 4442.
[35] K.M. Rabe, C.H. Ahn, J.-M. Triscone (Eds.), Physics of Ferroelectrics: A Modern Perspective, Springer-Verlag, Berlin Heidelberg, 2007.
[36] M.E. Lines, A.M. Glass, Principles and Applications of Ferroelectrics and Related Materials, Oxford University Press, Oxford, 2001.
[37] J.S. Tse, D.D. Klug, Phys. Rev. Lett. 67 (1991) 3559.
[38] J.S. Tse, D.D. Klug, Phys. Rev. Lett. 70 (1993) 174.
[39] R.T. Smith, F.S. Welsh, J. Appl. Phys. 42 (1971) 2219.
[40] J. Zhang, K.L. Yao, Z.L. Liu, G.Y. Gao, Z.Y. Sun, S.W. Fan, Phys. Chem. Chem. Phys. 12 (2010) 9197.
[41] H.J. Juretschke, Crystal Physics (Macroscopic Physics of Anisotropic Solids), W.A. Benjamin, Reading, MA, 1974.
[42] J.F. Nye, Physical Properties of Crystals, Clarendon Press, Oxford, 1957.
[43] P. Yeh, Introduction to Photorefractive Nonlinear Optics, Wiley and Sons, New York, 1993;
P. Gunter, J.P. Huignard, Photorefractive Materials and their Applications, Springer-Verlag, Berlin, I, 1988, II (1989).